Journal of Atmospheric and Solar–Terrestrial Physics 207 (2020) 105348

Contents lists available at ScienceDirect

Journal of Atmospheric and Solar-Terrestrial Physics

journal homepage: www.elsevier.com/locate/jastp

Application of the GPS reflected signals in tomographic reconstruction of the wet refractivity in Italy

Milad Jaberi Shafei [a], Masoud Mashhadi Hossainali [b,*]

[a] Faculty of Geodesy and Geomatics Engineering, K. N. Toosi University of Technology, Iran

[b] Department of Geodesy, Faculty of Geodesy and Geomatics Engineering, K. N. Toosi University of Technology, Iran

A R T I C L E I N F O

Keywords:
Refelectometry
Wet refractivity
GNSS
GNSS-R

A B S T R A C T

GPS troposphere tomography is one of the most powerful techniques used to extract 3D model of the water vapor and wet refractivity using the observations from local and regional GPS networks. In this technique each unknown parameter is related to the one 3D elements called voxels. This approach is a mixed-determined inverse problem because propagated signals do not pass through some of the voxels. As consequence, the design matrix has rank deficiency and unique solution cannot be reached. To this end, additional constraints are usually applied. In this research as an innovation, we utilized reflected signals from an air-borne reflectometry mission over Italy as additional constraint. According to the obtained results from four distinct parts in DOYs 158 & 160 of 2012, reflected signals help to remove or reduce the rank deficiency of our tomographic models. Due to the lack of radiosonde and radio occultation profiles, to validate the tomographic model results, GPS slant wet delay observations of singular GPS stations within the desired study areas are used as a measure for validation. Depending on the number of reflected and direct signals that we used in our reconstruction area, the range of bias in the developed models change from 1.6 to 6.9 mm. Moreover, the range of RMSE is 30–40 mm. The accuracy and precision of reconstructed images is adequate as far as the mean, minimum and maximum values of the slant wet delays in the test areas of this study are taken into account.

1. Introduction

GPS (Global Positioning System) signals passing through the neutral atmosphere are delayed and bent under the influence of the refractivity parameter. This results in lengthening of the geometric path of the ray, usually referred to as the tropospheric delay. Tropospheric delay is one of the major sources of error in positioning by GPS (Seeber, 2003). The refractivity parameter is mainly divided into dry and wet components. The dry component is relevant to pressure and temperature and can be determined in millimetric accuracy by the existing models, if the pressure and temperature are precisely known (Bevis et al., 1992). On the other hand, the wet component is related to the water vapor parameter that has a complex life cycle, including vertical and horizontal transport, mixing, condensation, precipitation and evaporation (Guerova et al., 2016). Consequently, due to the high temporal and spatial variation of water vapor, applied method should not only reconstruct this parameter in spatial domain but also consider its variations in time. Understanding the behavior of this parameter has significant contributes in determining the weather condition and also accurate estimation of tropospheric delay. GPS tomography is a technique which makes it possible to obtain 4D pictures from lower or medium troposphere by investigating the water vapor distribution in space and time (Bender and Raabe, 2007; Brenot et al., 2017; Guerova et al., 2016; Rohm and Bosy, 2009; Shangguan et al., 2013). Tomographic modeling has been successfully implemented in medicine (Beckmann and Spizzichino, 1987), geodynamics (Bourjot and Romanowicz, 1992), gas-tracing (Degaleesan et al., 2001) and ionosphere (Amerian et al., 2010). Troposphere tomography is implemented using a finite number of 3D elements (voxels) with assumed constant values (for the investigated quantity) to obtain the spatial and temporal distribution of the desired parameter using GPS signal as the input data (Adavi and Mashhadi-Hossainali, 2014; Adavi and Weber, 2019; Aghajany and Amerian, 2017; Bender et al., 2011; Haji-Aghajany et al., 2020; Rohm and Bosy, 2009; Yao and Zhao, 2016). Due to inappropriate distribution of the GPS stations and the satellites, some voxels are not sufficiently penetrated by the GPS signals. This characterizes the troposphere tomography as an ill-posed inverse problem (Adavi and Mashhadi-Hossainali, 2014; Bender et al., 2011; Brenot et al., 2020; Champollion et al., 2005; Rohm et al., 2014; Rohm

* Corresponding author.
E-mail addresses: m.jaberi@email.kntu.ac.ir (M.J. Shafei), hossainali@kntu.ac.ir (M.M. Hossainali).

https://doi.org/10.1016/j.jastp.2020.105348
Received 1 August 2019; Received in revised form 28 May 2020; Accepted 3 June 2020
Available online 11 June 2020

and Bosy, 2009; Song et al., 2006). To obtain a unique solution or to fix the rank deficiency of the problem, using additional constraints is inevitable. For this purpose, several methods have been implemented. Flores et al. (2001) utilized additional constraints through weighting unknown voxels by the neighboring ones (Flores, 1999). Hirahara (2000) applied horizontal and vertical smoothing equations to find the inverse solution (Hirahara, 2000). Flores et al. (2001) applied additional constraints in the form of a Kalman filter (Flores et al., 2001). Braun and Rocken (2003) used vertical profiles obtained by LIDAR radiometer from the Earth's surface up to 10 km as the required constraints (Braun and Rocken, 2003). Champollion et al. (2005) constrained their model using priori water vapor profiles from standard atmosphere and surface observations (Champollion et al., 2005). Bi et al. (2006) used averaged radiosonde observations in their study area during the desired time domain (Bi et al., 2006). Song et al. (2006) used Gauss weight function and vertical profiles derived from numerical weather prediction model as horizontal and vertical constraints, respectively (Song et al., 2006). Bender et al. (2011) applied surface observations to constraint the bottom layer of the model. Moreover, they constrained the most top layer of their model by a constant value (Bender et al., 2011). Xia et al. (2013) and Ye et al. used COSMIC occultation profiles as the required constraints (Xia et al., 2013; Ye et al., 2016). The idea of using Virtual Reference Stations (VRS) was proposed by Adavi and Mashhadi-Hossainali (2014). Heubelion et al. (2015 & 2019) used integrated water vapor (IWV) derived from Interferometry Synthetic Aperture Radar (InSAR) (Heublein et al., 2015; Heublein, 2019). Using an appropriate weighing method, Benevides et al. (2014) applied SWD observations calculated from the European Centre from Medium-Range Weather Forecasts (ECMWF) model (Benevides et al., 2014). Yao and Zhao (2017) used the radiosonde data to derive the maximum height of vertical axis and used the concept of non-uniform symmetrical division of horizontal voxels (Yao and Zhao, 2017). Zhao and Yao (2017,2018 & 2020) considered the signal rays penetrating from the model's side face as additional constraint to the tomographic model and solve the problem of the low utilization rate of global navigation satellite system (GNSS) observations (Zhao et al., 2020, 2018; Zhao and Yao, 2017). Benevides et al. (2018) used Atmospheric Infrared Sounder (AIRS) remote sensing data to initiate and update a 3-D tropospheric wet refractivity (Benevides et al., 2018). Shafie and Mashhadi-Hossainali (2018) used simulated ground based reflected signals as additional constraint to overcome the rank deficiency of the model (Shafei and Mashhadi-Hossainali, 2018). Zhao et al. (2019) utilized observations of GNSS receivers located outside the tomographic model region to participate in the establishment of a tomographic observation equation (Zhao et al., 2019). Haji-Aghajany et al. Utilized the Weather Research and Forecasting (WRF) model and the topography of the study area to reduce the deficiency of the model (Haji-Aghajany et al., 2020). This research is the first attempt to utilize reflected signals collected by an air borne mission in tomographic reconstruction of the wet refractivity and the analysis of the impact of these signals for improving the rank deficiency of model. To solve the tomography model many different approaches has been used such as using weighted and damped least-squares inversion with SVD (Champollion et al., 2005), the SVD and robust Kalman filter techniques to determine unknown parameters (Rohm et al., 2014), which based on the previous state and the correction to the measurement, combining weighted least-squares techniques with TSVD and 2D ray-tracing methods ((Möller, 2017)) and using simultaneous iterative reconstruction technique (Adavi and Mashhadi-Hossainali, 2014; Adavi and Weber, 2019) which we consider in this research.

In the next sections, tomographic modeling and related challenges are described. Reflected signals as an additional constrain is then discussed in brief. Next, regularization method that we utilized in this paper is introduced. Finally, data sets, numerical results and validation of the reconstructed images are completely given. Concluding remarks and suggestions are given last.

2. Tomographic modeling

Troposphere tomography is based on exploiting GPS signals for reconstructing 3D or 4D images of some atmospheric parameters such as refractivity. This idea is based on the fact that transmitted signals are delayed and bent through their path due to the changes of pressure, temperature and relative humidity. The corresponding Slant Total Delay (STD) is determined by (Bevis et al., 1992):

$$STD = 10^{-6}\int_{s} N(s)ds + (S-G) \approx 10^{-6}\int_{s} N(s)ds \tag{1}$$

where s is the signal path between satellite and receiver and N is the refractivity parameter. The term $S-G=\int_s ds - \int_g ds$ is the geometric delay that describes extra path of transmitted GPS signals due to their bending. In troposphere tomography this part is neglected and the signals' path is assumed to be straight (Adavi and Mashhadi-Hossainali, 2014; Guerova et al., 2016; Rohm and Bosy, 2009; Troller et al., 2006). Eq. (1) is usually expressed in terms of the Slant Wet and the Slant Hydrostatic Delays (SWD & SHD). SHD can be computed with a few millimeters accuracy using global troposphere models (Bevis et al., 1992). Consequently, SWD is determined by the subtraction of STD from SHD as given bellow:

$$SWD = STD - SHD = 10^{-6}\int N_w ds \tag{2}$$

N_w is the wet refractivity parameter in Eq. (2). This is a nonlinear integral equation and should be set up for the GPS signals at every measurement epoch (Guerova et al., 2016). To this end, first, the mathematical model is linearized by discretizing the refractivity field into a 3D gridded mesh of elements with limited dimensions (regarding to the spatial variation of the desired parameter) called voxels. Next, with such assumptions Eq. (2) is substituted with the finite series as follows:

$$SWD_i = 10^{-6}\sum N_{wj}\Delta s_j \tag{3}$$

In equation above index j represents the voxel that the i th signal passes through it and parameter Δs_j is the corresponding signal length. In matrix notation, the simultaneous system of observation equations of type Eq. (3) is formed as bellow:

$$b = Am \tag{4}$$

where A is referred to as the design matrix of tomographic model with $m \times n$ dimensions (Adavi and Mashhadi-Hossainali, 2014; Rohm and Bosy, 2009):

$$\mathbf{A} = \begin{bmatrix} d_{11} & . & . & . & d_{1n} \\ d_{21} & . & . & . & d_{2n} \\ . & . & . & . & . \\ . & . & . & . & . \\ d_{m1} & . & . & . & d_{mn} \end{bmatrix} \tag{5}$$

m is the number of SWD observations and depends on the number of GPS stations and the time response of the tomographic model, n is the number of unknowns (voxels) and d_{ij} is the length of signal i in voxel j. Due to the variation of satellites' and tracking points' relative position in each epoch, elements of the design matrix are not constant. In tomographic model, if the signal does not intersect a voxel, the related element is set to zero. Moreover, the refraction of the signal is ignored (Adavi and Mashhadi-Hossainali, 2014; Champollion et al., 2005; Rohm and Bosy, 2009). To come up with a unique solution, transmitted signals should pass necessarily through all of the model's elements. Since the GPS space segment is not optimized for this purpose, some of the voxels are not covered by GPS signals while others might be over constrained. Consequently, troposphere tomography is a mixed-determined inverse problem (Menke, 2018). Therefore, to completely constrain the model or to fix the rank deficiency of design matrix, adding extra information/observations is necessary.

3. Reflectometry constraints & analyzing their impact on the model

This research applies GPS reflected signals (GPS-R) as additional data to constrain the tomographic model and remedy the rank deficiency of the problem. GPS-R is a bi-static radar system in which the transmitter and receiver are separated by a significant distance. The first concept was investigated by Martin-Neira (1993) as a method to densify the earth observations in a low cost efficient way. For this purpose, an antenna pointing to transmitter receives the so-called direct signals and an antenna pointing to the surface gathers the signals scattered from the surface of the Earth (reflected signals). By now, reflected signals are used for specific applications. The reflected signals were used to analyze the temporal variation of the sea surface and lake level in many researches (Cardellach et al., 2011; Rius et al., 2010; Ruffini et al., 2004; Semmling et al., 2011). In addition, they were utilized to extract the surface roughness and parameters such as: the soil moisture and ice properties by analyzing the Delay Doppler Maps (DDMs) extracted from the waveforms (Cardellach et al., 2011; Katzberg et al., 2006; Larson et al., 2013; Rius et al., 2012; Rodriguez-Alvarez et al., 2010; Zavorotny and Voronovich, 2000). The particular advantage of this technique is the dense temporal and spatial coverage not only limited to a single measurement point or a non-repetitive transect as with using classical GPS buoys (Roussel et al., 2014). Pallarés et al. investigated tomographic modeling of ionosphere over the oceans using GPS-R data, collected by Low Earth Orbiter mission (LEO), besides other data such as the occultation and Total Electron Contents (TECs) (Pallarés et al., 2005).

The number and spatial distribution of GPS stations are usually not suitable for troposphere tomography. Accordingly, the GPS signals alone fail to constrain the model, especially in the lower voxels. Here, we use only the reflected signals to investigate the impact of GPS-R on fixing this problem. To apply such additional observations, the specular points' position (the geometric position of reflection points assuming that the reflections are specular) is considered (Roussel et al., 2014; Shafei and Mashhadi-Hossainali, 2018). Then, the reflected signals' path are added to the model regarding the position of the transmitter, receiver and specular points.

We use the model space resolution matrix ($\mathbf{R}_m$) in order to analyze the impact of reflected signals on the rank deficiency of the problem. The concept of resolution matrix is an appropriate way to characterize the bias in a discrete inverse problem. On the assumption that there are no errors in the input data, $\mathbf{R}_m$ analyzes how close is the inverse solution to an original model (Adavi and Mashhadi-Hossainali, 2014):

$$\mathbf{R}_m = \mathbf{V}_p \mathbf{V}_p^T \tag{6}$$

here, p is the number of singular values that are effectively non-zero and V is the right singular matrix of the coefficient matrix A. If A is full rank, i.e. the elements of the tomographic model are constrained by utilized signals (GPS and reflected signals), the model null space is trivial and $\mathbf{R}_m$ is an identity matrix. Otherwise, the resolution matrix is asymmetric with some diagonal elements that are either zero or close to zero which means the parameters that are correspondent to such elements are poorly reconstructed by the inverse solution (R. Aster, B. Borchers, 2005).

4. Regularization method

Iterative regularization methods are preferred approaches when a large scale inverse problem such as tomographic modeling is concerned (Elfving et al., 2010). In this paper, after fixing the rank deficiency of the problem, Landweber regularization method is utilized. Landweber is a classic iterative regularization technique which seeks a regularized solution by solving the optimization problem $\min_{\mathbf{m}} \|\mathbf{b} - \mathbf{A}\mathbf{m}\|_2^2/2$. The classical form of this algorithm suggests an update to sought solution by (Landweber, 1951):

$$\mathbf{m}^{k+1} = \mathbf{m}^k + \lambda_k \mathbf{A}^T \left(\mathbf{b} - \mathbf{A}\mathbf{m}^k\right) \tag{7}$$

where $\mathbf{m}$ is the vector of the desired unknowns and λ is the relaxation parameter. To insure the convergence, λ should be in the range of $0 < \lambda < {}^2/_{\sigma^2_{\max}}$. Here, $\sigma^2_{\max}$ is the largest eigenvalue of the design matrix (R. Aster, B. Borchers, 2005).

λ can be obtained by different approaches such as linear $\psi_1 \& \psi_2$ based relaxation strategies or modified $\psi_1 \& \psi_2$ strategies (Elfving et al., 2010). $\psi_1 \& \psi_2$ strategies are indeed able to dampen the influence of the noise-error, as desired. Moreover, initial convergence is almost identical with much better damping of the noise propagation: once we reach the minimum in the error histories, then the error only increases slowly (Elfving et al., 2010).

In this study, to enrich relaxation parameter we prefer to use the modified Ψ_2 method which accelerates the convergence (Elfving et al., 2010). To reach the optimum number of iterations, due to the lack of radiosonde and radio occultation profiles within the desired time domain, at each iteration, the slant tropospheric delays derived from tomographic models and the GPS stations which are not included in tomographic modeling were compared in different elevation angles. The iterations stop when calculated RMSE (Eq. (8)) of this comparison is minimized. Moreover, for more analysis the bias is calculated by Eq. (9):

$$RMSE = \sqrt{\frac{1}{N}\sum_{i=1}^{N}\left(\mathrm{mod}^i - cal^i\right)^2} \tag{8}$$

$$bias = \frac{1}{N}\sum_{i=1}^{N}\left(\mathrm{mod}^i - \mathrm{cal}^i\right) \tag{9}$$

where mod^i refers to the parameter that is extracted from tomographic model and cal^i is the corresponding one calculated using the Bernese software at the test stations mentioned above.

5. Numerical results and conclusions

In this section, first, the study area is introduced. Next, the dataset is briefly described and the strategies applied for calculating slant delays for both GPS stations and reflected signals are explained. The impact of adding reflected signal as constraints on the design matrix of the tomographic model is then given. To this end, the concept of resolution matrix is used. Finally, to evaluate the performance of the model; slant delays produced by the reconstructed model are compared with slant delays extracted from isolated GPS stations within each of the study areas.

5.1. Study area and datasets

At present, due to the limitation of GPS-R missions, available data is limited to particular areas at specific times. These missions are not planned for GPS metrology. Besides, ground based GPS-R missions are usually conducted in the areas that are far from permanent GPS stations. Considering mentioned limitations, an air-borne mission has been preferred. Since reflectometry data together with the GPS and synoptic stations are available in some part of Italy, this area is adopted as the study region. The GPS-R data has been provided by the GEOHALO (High Altitude Long Range) mission. The mission was designed and commissioned in a joint collaboration between the German research institute Geo Forschungs Zentrum (GFZ) and the Institute de Ciències de l'Espai for atmospheric geophysics research. With the aim of altimetry using signals reflected from the surface of the sea, it covered Mediterranean region. This four days mission also included gravimetry, magnetometry, laser altimetry and GPS positioning surveys (Semmling et al., 2014).

National Institute of Geophysics and Volcanology (INGV) in Italy established the Italian Permanent GPS Network RING (RETE INTEGRATA NAZIONALE GPS) in 2004. At present, the network consists of 180 GPS stations. It is used for monitoring the convergence of the Arabian and Eurasia plates across the western Mediterranean region as a high rate deformation zone. In this research some GPS stations of the RING network are utilized.

Considering both the GPS stations' dispersion and availability of reflected signals, the time period of this study is limited to 2 h (DOYs 158 and 160 of the year 2012). We only use the specular points' (geometric) positions because the other datasets are not relevant to the aim of this research. Fig. 1 represents the distribution of GPS stations and reflected signal positions in this area.

For the GPS stations' signals (here after referred to as the direct signals), first, ZTDs are computed using the Bernese GPS software (Dach et al., 2007). Then, ZWDs are derived from the subtraction of the ZHDs from ZTDs. We used Saastamoninen's model for computing the ZHDs. This is done using the precise meteorological parameters that are made available to this research (Bevis et al., 1992). Temperature, pressure and relative humidity are recorded at the synoptic stations surrounding the study area of this research (see Table 1). Therefore, they are interpolated at the GPS positions. Using the GMF mapping function calculated ZWDs are then transferred to SWDs.

For reflected signals, SWD is computed using two different methods: In the first approach, we used the ray tracing algorithm (Eresmaa and Järvinen, 2006) and the ECMWF model. ECMWF is a 3D gridded representation of the atmospheric condition in the form of pressure layers located at different heights. The spatio-temporal resolution of the data used in this study is 3 km and 1 h, respectively. To calculate SWDs for reflected signals, they are divided into two parts. The first part is limited to the signal path between the satellite and the specular point positions

Table 1
Synoptic stations that are used in this research.

Name of station	Geographic Position (in decimal degrees)	
	Latitude	Longitude
VITERBO PRATICA	42.430	12.064
VINGA	42.083	12.217
DE VALLE	42.432	14.181
PESCARA	42.00	15.00
TERMOLI	41.99	12.741
GUIDONIA	41.799	12.595
CIAMPINO	41.804	12.251
FIUMICINIO	41.542	12.909
DE MARE	41.633	13.300
GIOIA DEL COLLE	41.659	12.445
FROCINONE	41.061	14.082
GRAZZANISE	41.541	15.718
AMENDOLA	41.133	16.767
BARI	40.917	12.95
PONZA ISLAND	40.55	14.25
CAPRI ISLAND	40.768	16.933

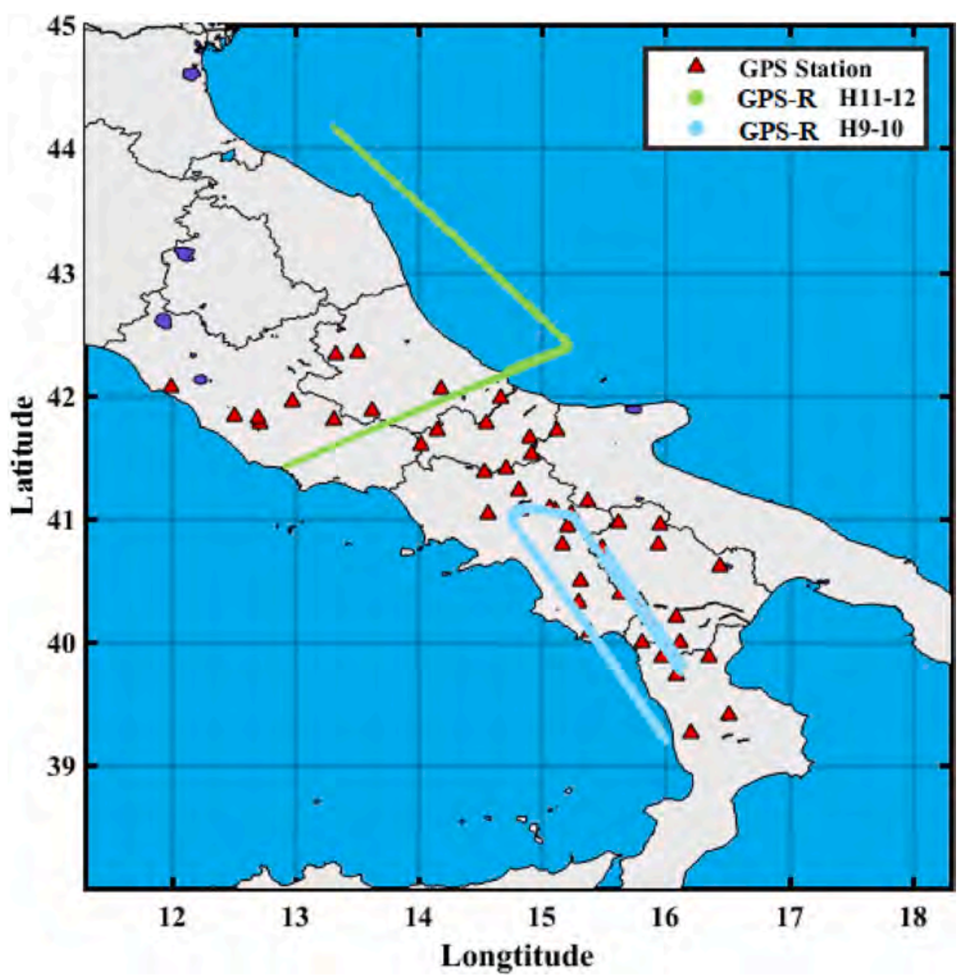

Fig. 1. Study area: the blue and light green tracks illustrate the specular points' locations at DOYs 158 & 160 for the time periods 11–12 & 9–10 in GPS time (H11–12, H9-10), respectively.

(SWD1) and the other one starts from this point to the receiver position (SWD2). Therefore, for a reflected signal SWD is the sum of the both parts (SWD=SWD1+SWD2). Computation of SWDs is limited to the height of the tomographic model. We refer to this method as the complete model approach. In the second approach, troposphere is divided into two parts: common and differential troposphere. In GPS-R, differential and common troposphere refer to the parts of troposphere that are below and above the down looking antenna, respectively (Fabra, 2013). Here, the differential part is only taken into account. Consequently, the reflected signal path is limited to the signal path between a receiver and specular point, and; from this point to the satellite position which is cut off in receiver's height. To compute wet delays, the total differential tropospheric delay is firstly computed using the following equation:

$$\rho_{tropo} = 2(2.3 / \sin(\varepsilon))(1 - \exp(H_R - h_{scale})) \tag{10}$$

here, ε is the elevation angle of the down looking antenna at the specular point and h_{scale} is the scale height of the troposphere (Fabra, 2013). To separate the wet component from the total differential delay the ratio of the slant wet to the slant total delay in the direction of defined reflected signal path, is calculated using the method of ray tracing. Differential wet delays are derived by multiplying this ratio to the delay computed by Eq. (10). Here, we refer to this method as the differential model approach.

5.2. Tomography model

In this study, the time response of the tomographic model is 1 h. In other words, unknowns are considered to be constant in this time resolution. The vertical resolution of the model is 500 m from the surface to the 4 km height and then is reduced to 1000 m up to the height of 10 km from the surface of the Earth, where the wet refractivity and the water vapor parameters are considered to be zero. The horizontal resolution selected for this model is based on the distribution of GPS stations and the available reflected signals. Table 2 represents the GPS stations that are used in this research. It should be noted that horizontal grid size is not much smaller than the mean distance of the GPS stations. In addition, to design the tomographic model; topography of the study area is also taken into account. In this study, due to the limitations mentioned for datasets, four distinct areas are considered for tomographic modeling (see Fig. 2). As result, the horizontal resolution of these models are different for each of the selected areas. The horizontal dimensions of the model elements are: 25 × 30, 35 × 35 and 33 × 25 in kilometers at Area1, Area2, Area3 and Area4, respectively and the mean distance of GPS stations in these areas are: 26 km, 14.7 km, 35.1 km and 30.3 km as well.

Table 2
The GPS stations of this study.

Name of station	Geographic Positions (in decimal degrees)		Applied area
	Latitude	Longitude	
CAFE	41.03	15.24	Area 1
GRO1	41.07	15.1	Area 1
GROT1	41.07	15.06	Area 1
MCRV	40.78	15.17	Area 1
MFUS	41.06	14.83	Area 1
PSB1	41.22	14.81	Area 1
SGTA	41.14	15.37	Area 1
SNAL	40.93	15.21	Area 1
MCEL	40.33	15.8	Area2
SIRI	40.18	15.87	Area2
SLCN	40.39	15.63	Area2
CERT	41.95	12.98	Area3
GUAR	41.79	13.31	Area3
INGR	41.83	12.51	Area3
RDPI	41.76	12.71	Area3
RMPO	41.81	12.7	Area3
VVLO	41.87	13.62	Area3/Area 4
CERA	41.6	14.02	Area4
LPEL	42.05	14.18	Area4
RNI2	41.7	14.15	Area4

Since the height of the plane varies from 3000 to 4500 m, reflected signals can only constrain the lower layers of the model. Fig. 3 illustrates the position of the airborne receiver with respect to the model and the topography of the study areas Area1 & Area2.

5.3. Impact of reflected signals on the tomographic model

Considering the direct and reflected signals' path, the design matrix of the tomographic model is made using ray tracing technique. The specular point positions are taken from the given data set. To this end, the satellites', receivers' and specular points' positions should be in the same local frame. Each row of the matrix is derived through the intersection of the ray and voxel plane equation annalistically.

Results (see Fig. 4) show that when GPS signals are the only data utilized in tomographic modeling, in all study areas, the model null space is nontrivial and unique solution is not available. When reflected signals are added to the model as additional constraints, the rank deficiency of the design matrix is completely fixed (Area1 & Area2) or improved (Area3 and Area4). In the former case, the rank deficiency of the tomographic model is completely removed while in the latter case the deficiency of the design matrix improved by 50% and 60%, respectively.

Computed model space resolution matrices (R_m) are also given in Figs. 5 and 6. For the test areas Area1 & Aea2 (see Fig. 5), resolution matrices are non-diagonal when GPS data are the only inputs. The off-diagonal elements are the model parameters that are smeared when the solution is derived. For these areas, resolution matrices become diagonal when the reflected signals are added. In other words, all of the unknown parameter can be derived. Nevertheless, application of these added constraints cannot remedy the rank deficiency of the problem in the remaining areas (see Fig. 6).

5.4. Validation of the reconstructed images

A comparative analysis on the estimated and modeled slant delays is used for validating proposed models. Application of this method is inevitable due to the lack of radiosonde and radio occultation profiles within the study time domain. The comparison is made between the slant tropospheric delays computed using tomographic models and the check stations' GPS data. GPS slant delays were derived by processing the corresponding data using Bernese software. Processing strategy was similar to what we used for the direct signals. GPS stations, GROT1 in Area1 and MCEL in Area2 (two test areas where models were fully constrained by reflected signals) have been selected for this purpose (see yellow triangle in Fig. 2). GPS data of these stations did not contribute in the reconstruction of the model. Moreover, exclusion of these data does not change the rank deficiency and resolution of the model. The GMF mapping function is used for projecting ZWDs to the desired directions (Böhm et al., 2006). SWD residuals are computed by subtracting GPS-SWDs from the their values derived from tomographic models. further details on this comparison are given in Fig. 7 for the complete and Fig. 8 for the differential model approaches.

According to Figs. 7 and 8, deviation of the obtained results represents that the accuracy of reconstructed slant delays is better when the elevation angle is high. This accuracy is decreased when the elevation angle is reduced. It is well known that the noise of reflected signals is larger than the noise of direct ones. The contribution of reflected signals in the lower layers of tomographic models is higher as compared to the upper parts. As the result, the accuracy of reconstructions is not the same at the upper and lower parts of a model. Table 3 reports on the overall accuracy and precision of proposed models.

A reconstructed image is supplied more by reflected signals when direct signals fail to properly constrain the model. This also happens

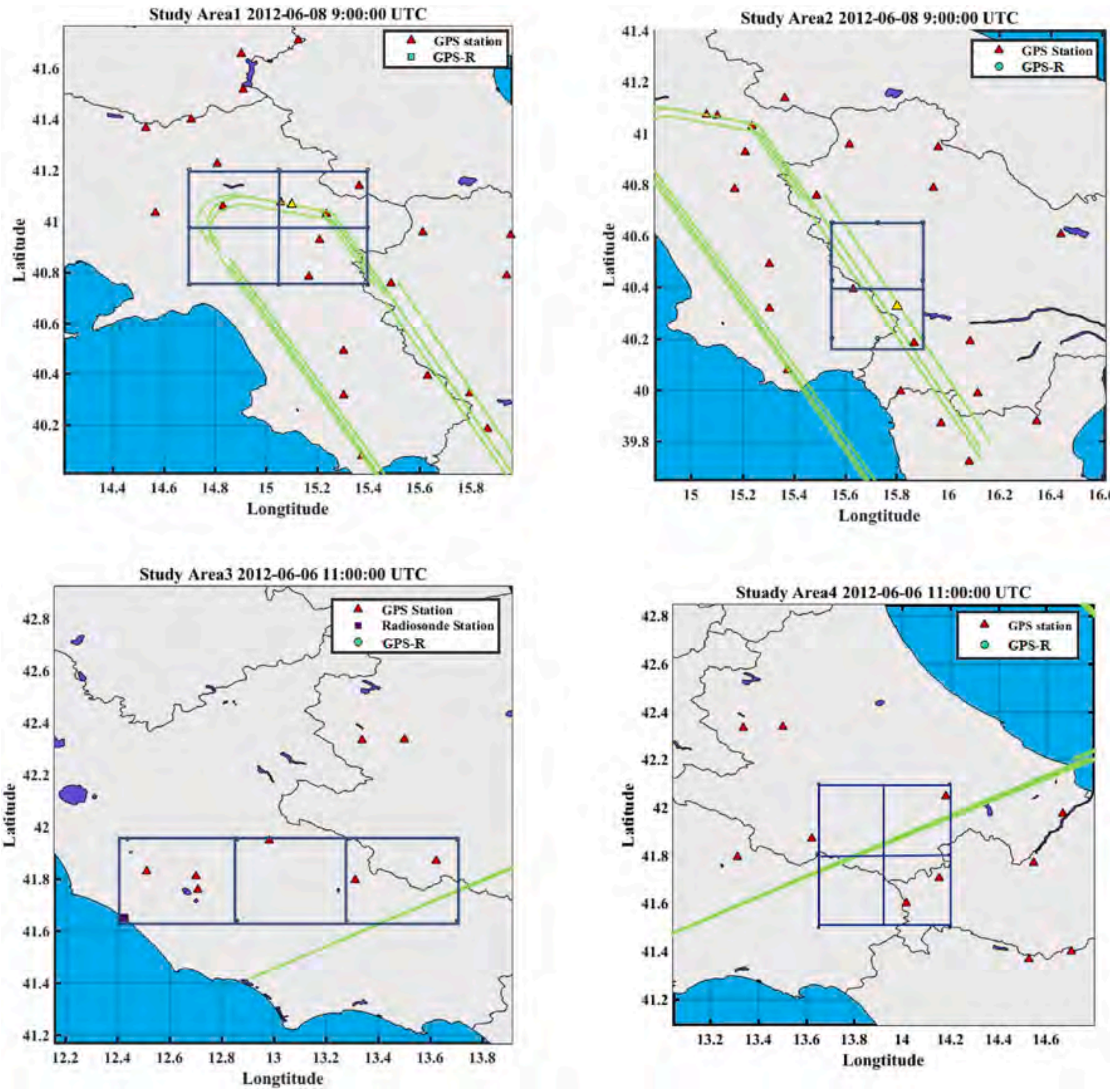

Fig. 2. The distribution of GPS stations, reflected signals and the tomographic models for the selected areas, DOYs 158 & 160.

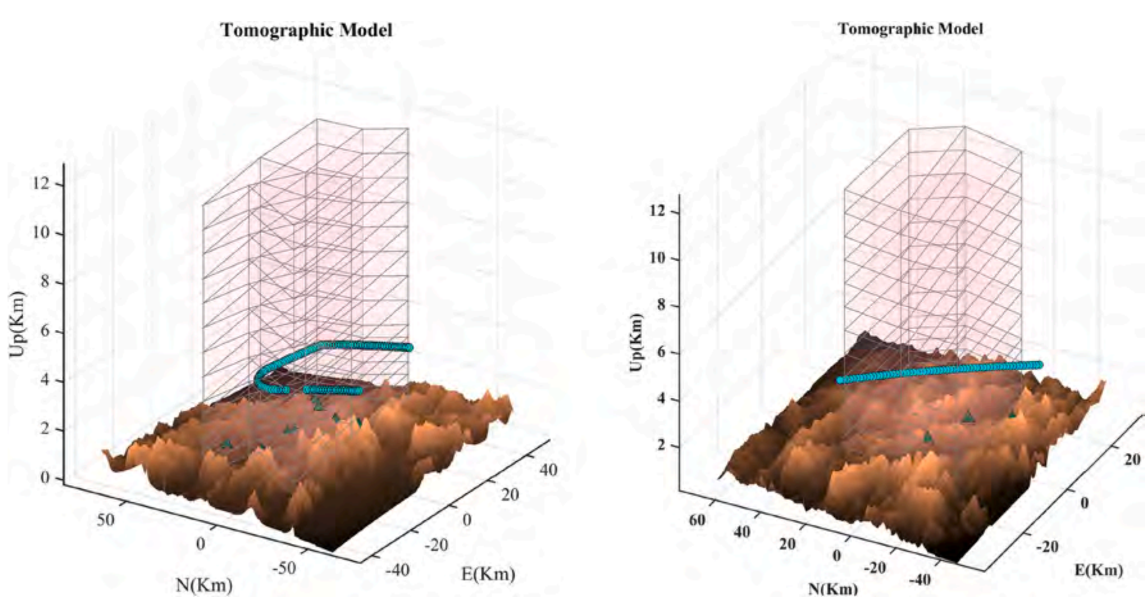

Fig. 3. Distributions of the GPS stations and the airborne receiver positions with respect to the topography and the tomographic models in: (a) Area1 & (b) Area2.

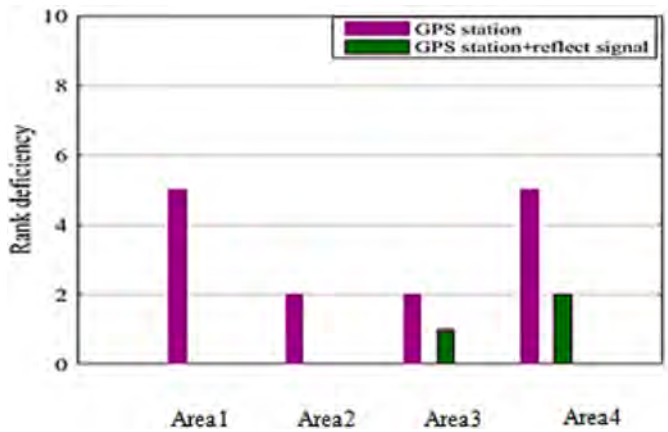

Fig. 4. The rank deficiency of tomographic model for (a) using only GPS data, given bars in purple and (b) using GPS and GPS-R data, given bars in green.

when the number of GPS stations is not sufficient and/or they are located next to the boundary of a model. This situation is seen in the distribution of GPS stations in Area 2 (see Fig. 2). As the result the overall bias of the tomographic model is larger in this area. Table 3 also shows that the computed mean bias is almost independent of the used method for estimating SWDs on reflected signals. In other words, the accuracy of SWDs computed from the ECMWF model is almost similar to the accuracy of SWDs that are computed by Eq. (10). Large differences in the accuracies of reconstructed results for high and low elevation angles not only imply that the estimation of tropospheric delay on reflected signals is a challenging problem but also suggests that the contribution of reflected data should be limitted to the minimum number of measurements required for resolving the rank deficiency of the problem. The later assertion is seen from the comparison of RMSEs in Area 1 & Area 2. Since the contribution of reflected data in the reconstructed SWDs in Area 2 is less than the direct ones, estimated RMSE in this area is smaller than the estimate of this quantity in Area 1. Finally, reconstructed images are reasonable as far as the mean, minimum and maximum values of the slant wet delays are concerned. Table 4 provides the corresponding details.

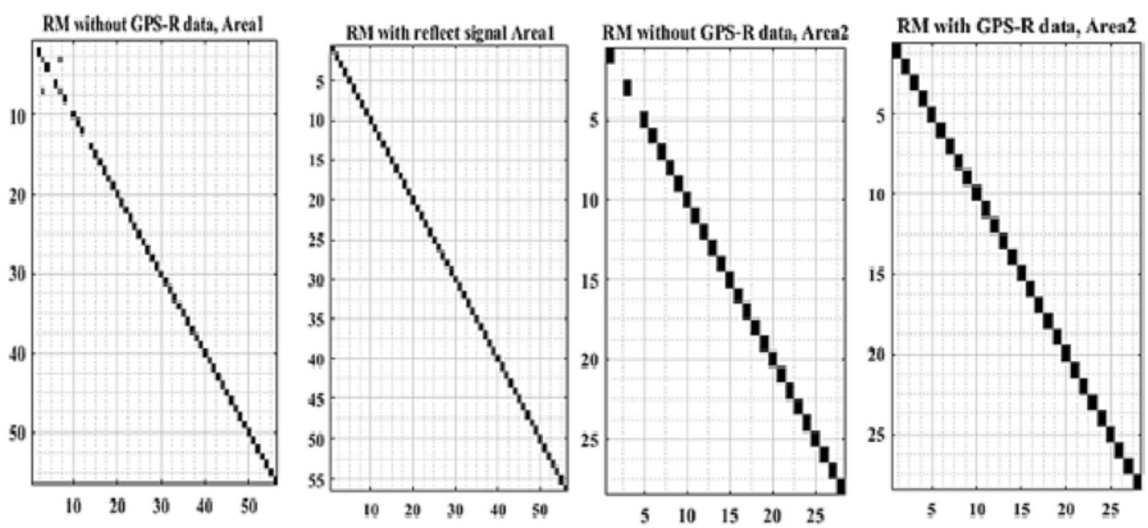

Fig. 5. Resolution matrices in Area1 & Area2: DOY 158, Epoch 9.

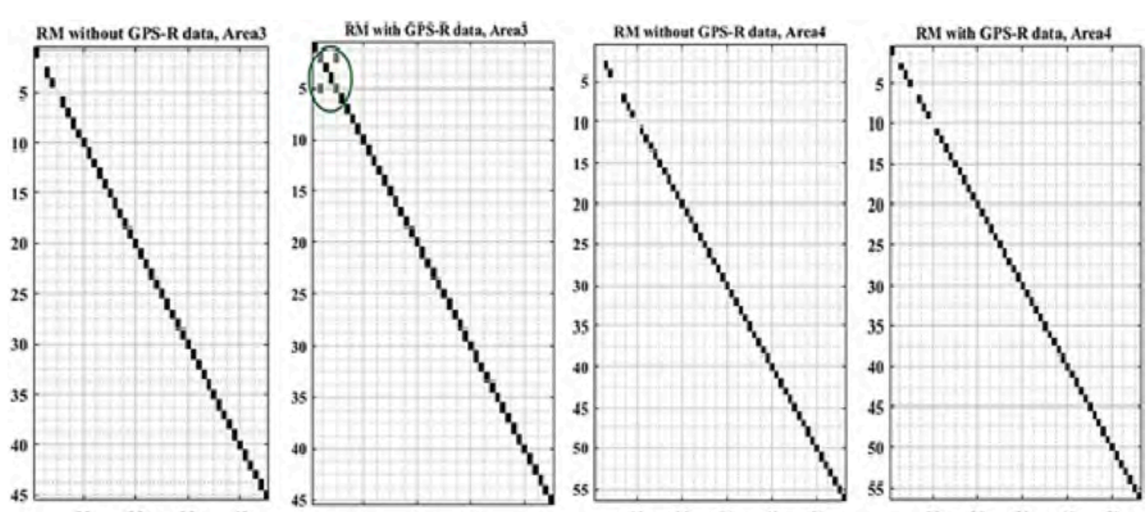

Fig. 6. Resolution matrices in Area3 & Area4: DOY 160, Epoch 11 (green circle in resolution matrix for Area3 represent that the resolution matrix is not diagonal and those parameters cannot be derived from the model).

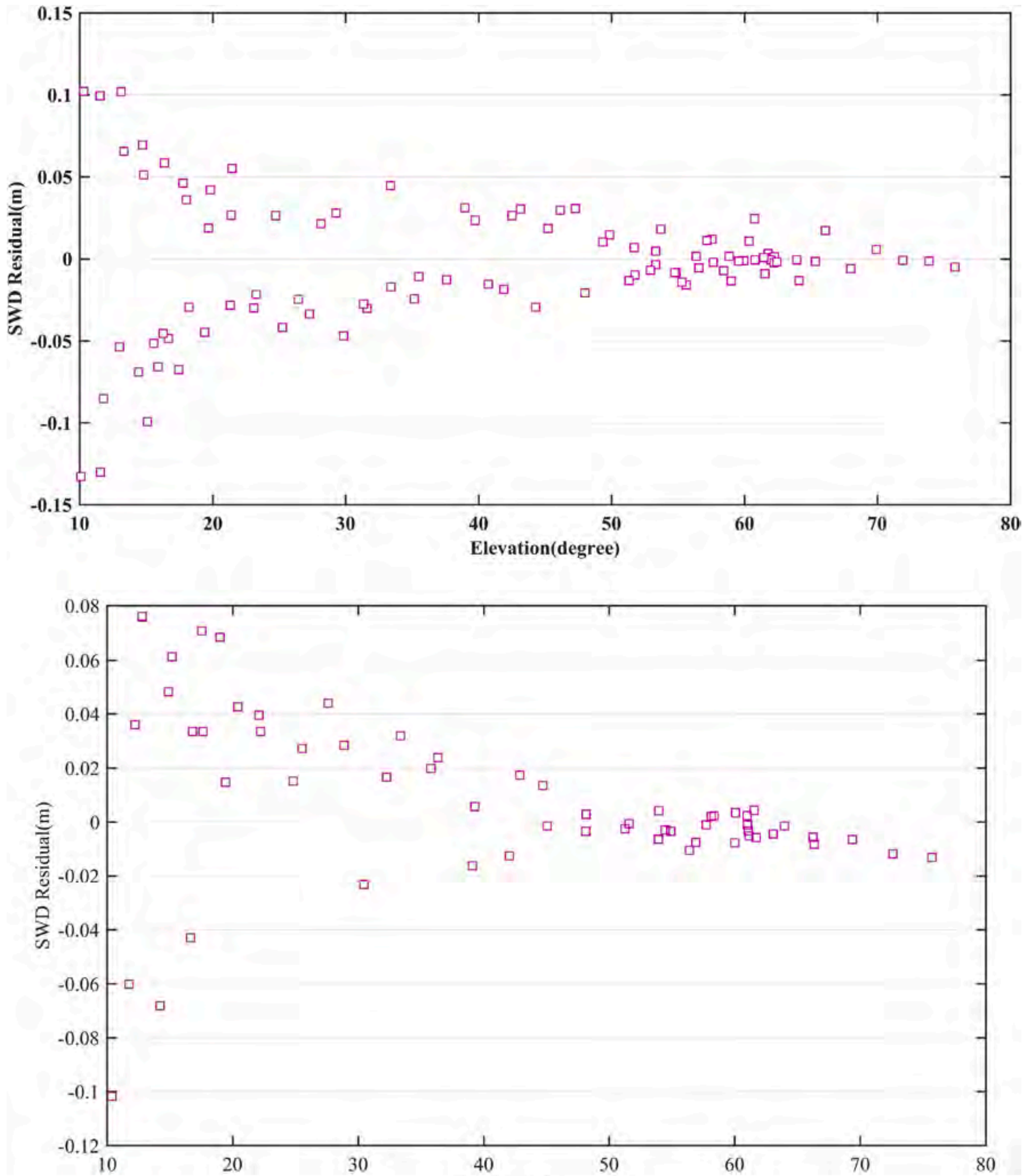

Fig. 7. Validation of the reconstructed wet refractivity images: (a) Area1 and (b) Area2. Residuals are computed using the complete model approach, DOY 158, H9-10.

6. Conclusions and suggestions

This research is the first attempt to the application of reflected signals from aerial mission in troposphere tomography. The required GPS, GPS-R and meteorological data available in parts of Italy are used for this purpose. Some of the RING GPS stations in Italy, the GOLD-RTR data from the HALLO reflectometry mission and synoptic records are utilized as data sources. the adequacy of the tomographic models in reconstructing the unknowns (the wet refractivity) is checked using the concept of the model space resolution matrix. Obtained results show that reflected signals can successfully constrain the model in two parts of the study area while the rank deficiency of the model can be only reduced in the others. This is mainly because the HALLO mission was not planned for GPS met applications like the present research. According to the obtained results, in the test areas Area 3 & Area 4 the rank deficiency of the problem is improved by 50% and 60%, respectively; while in Area 1 and Area 2, adding reflected to the direct GPS signals supports the uniqueness of the sought solution. The accuracy of the tomographic model is checked by two GPS stations in fully constraint models, i.e. in the test areas Area1 & Area2. Mean bias and RMSE of the slant wet delays computed from the analysis of GPS data and reconstructed images are the statistical measures used for evaluating the obtained results. In Area1, mean bias is about 3 mm and the RMSE of the reconstructed SWDs is about 4 cm. In Area 2, mean bias and RMSE change to 7 mm and 3 cm, respectively. According to this study, in order to reduce the existing bias in the tomographic images; the contribution of reflected data should be limited to the minimum number of measurements required for resolving the rank deficiency of the problem. Two methods

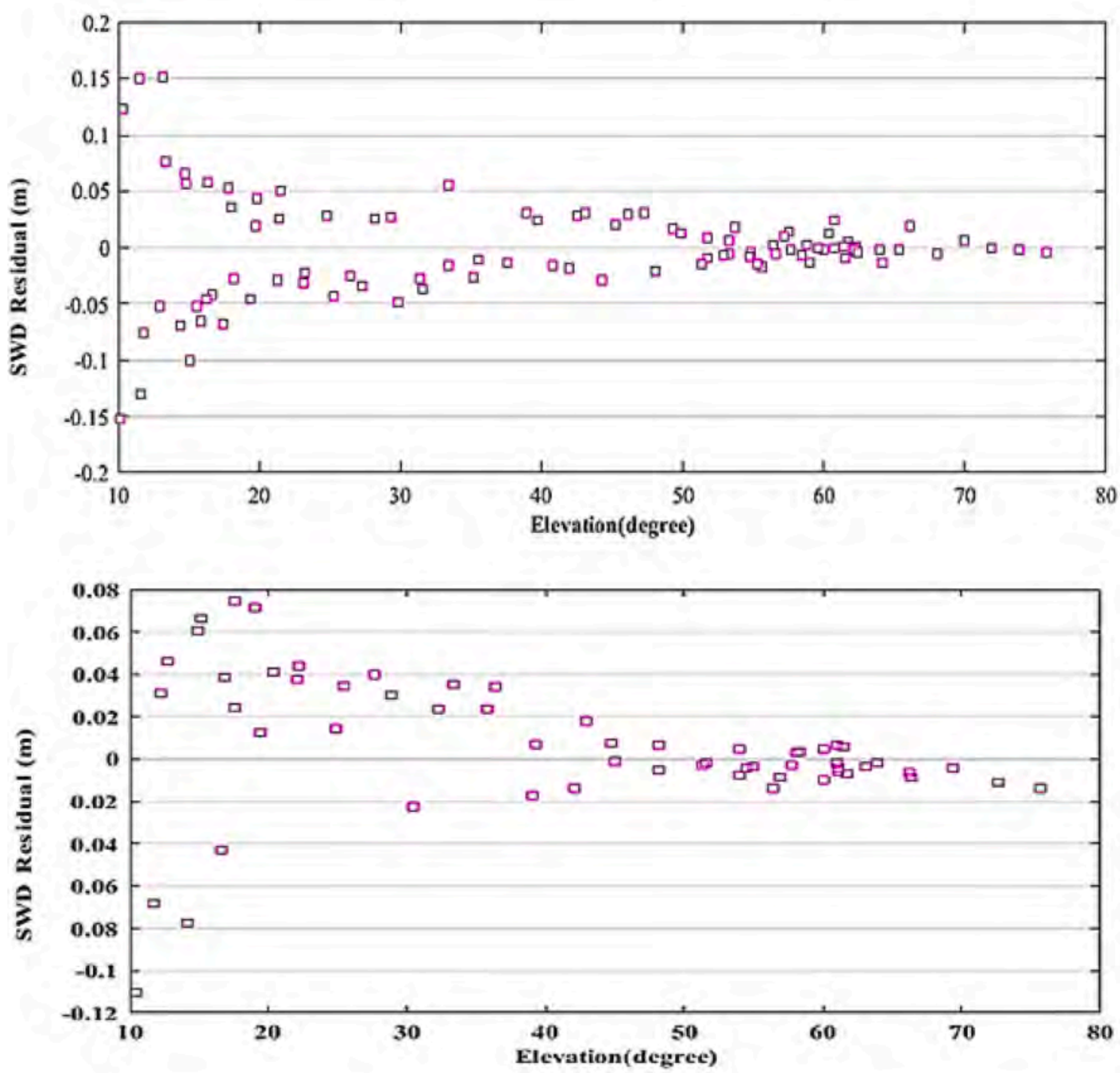

Fig. 8. Validation of the reconstructed wet refractivity images: (a) Area1 and (b) Area2. Residuals are computed using the differential model approach, DOY 160, H9-10.

Table 3
Statistical measures computed for the analysis of reconstructed images for the wet refractivity in Area 1 and Area 2. Given results are in mm.

Statistical Measure	Experiment Area (Complete Model Approach)		Experiment Area (Differential Model Approach)	
	Area 1	Area 2	Area 1	Area 2
Mean bias	−2.9	6.5	−1.7	6.9
RMSE	40.2	30.2	44.9	32.9

Table 4
Some statistics on the slant wet delays computed using reconstructed image. Given results are in meter.

GPS Test Station (Area)	Computed SWDs (m)		
	Minimum	Mean	Maximum
GROT (AREA1)	0.2354	0.4707	1.2829
MCEL (AREA2)	0.2066	0.4104	1.1258

are used for computing the slant wet delays on reflected signals. The accuracy of both approaches are similar at least in the experiment areas of this research. The accuracy and precision of reconstructed images is adequate as far as the mean, minimum and maximum values of the slant wet delays in the test areas of this study are taken into account. It is suggested that the troposphere tomography using reflected signal as an additional constraint must be tried in the missions that are planned for this purpose. Moreover, in serve weather condition this method should be checked and evaluated.

Acknowledgements

The authors would like to acknowledge the Institut de Ciències de l'Espai for providing the GOLD-RTR part of the HALO mission data to this research. We also appreciate Dr. Fran Fabra and Dr. E. Cardellach for their valuable suggestions and comments. The authors are grateful to the INGV RING Working Group for providing the observation files of the RING network in Italy.

References

Adavi, Z., Mashhadi-Hossainali, M., 2014. 4D tomographic reconstruction of the tropospheric wet refractivity using the concept of virtual reference station, case study: northwest of Iran. Meteorol. Atmos. Phys. 126, 193–205.

Adavi, Z., Weber, R., 2019. Evaluation of virtual reference station constraints for GNSS tropospheric tomography in Austria region. Adv. Geosci. 50, 39–48.

Aghajany, S.H., Amerian, Y., 2017. Three dimensional ray tracing technique for tropospheric water vapor tomography using GPS measurements. J. Atmos. Sol. Terr. Phys. 164, 81–88.

Amerian, Y., Hossainali, M.M., Voosoghi, B., Ghaffari, M.R., 2010. Tomographic reconstruction of the ionospheric electron density in term of wavelets. J. Aero. Sci. Technol. 7, 19–29.

Aster, R., Borchers, B., C T, 2005. Parameter Estimation and Inverse Problems. Elsevier, New York.

Beckmann, P., Spizzichino, A., 1987. The Scattering of Electromagnetic Waves from Rough Surfaces. Artech House, Inc., Norwood, MA, p. 511, 1987.

Bender, M., Raabe, A., 2007. Preconditions to ground based GPS water vapour tomography. Annales Geophysicae, pp. 1727–1734.

Bender, M., Dick, G., Ge, M., Deng, Z., Wickert, J., Kahle, H.-G., Raabe, A., Tetzlaff, G., 2011. Development of a GNSS water vapour tomography system using algebraic reconstruction techniques. Adv. Space Res. 47, 1704–1720.

Benevides, P., Catalao, J., Miranda, P.M., 2014. Experimental GNSS tomography study in Lisbon (Portugal). Física Tierra 26, 65–79.

Benevides, P., Catalao, J., Nico, G., Miranda, P.M.A., 2018. 4D wet refractivity estimation in the atmosphere using GNSS tomography initialized by radiosonde and AIRS measurements: results from a 1-week intensive campaign. GPS Solut. 22, 91.

Bevis, M., Businger, S., Herring, T.A., Rocken, C., Anthes, R.A., Ware, R.H., 1992. GPS meteorology: remote sensing of atmospheric water vapor using the Global Positioning System. J. Geophys. Res. Atmos. 97, 15787–15801.

Bi, Y., Mao, J., Li, C., 2006. Preliminary results of 4-D water vapor tomography in the troposphere using GPS. Adv. Atmos. Sci. 23, 551–560.

Böhm, J., Niell, A., Tregoning, P., Schuh, H., 2006. Global Mapping Function (GMF): a new empirical mapping function based on numerical weather model data. Geophys. Res. Lett. 33.

Bourjot, L., Romanowicz, B., 1992. Crust and upper mantle tomography in Tibet using surface waves. Geophys. Res. Lett. 19, 881–884.

Braun, J.J., Rocken, C., 2003. Water vapor tomography within the planetary boundary layer using GPS. International Workshop on GPS Meteorology. Citeseer.

Brenot, H., Rohm, W., Kačmařík, M., Möller, G., Sá, A., Tondaś, D., Rapant, L., Biondi, R., Manning, T., Champollion, C., 2017. Cross-validation of GPS Tomography Models and Methodological Improvements Using CORS Network. EGU2017-7078. EGU, poster.

Brenot, H., Rohm, W., Kačmařík, M., Möller, G., Sá, A., Tondaś, D., Rapant, L., Biondi, R., Manning, T., Champollion, C., 2020. Cross-comparison and methodological improvement in GPS tomography. Rem. Sens. 12, 30.

Cardellach, E., Fabra, F., Nogués-Correig, O., Oliveras, S., Ribó, S., Rius, A., 2011. GNSS-R ground-based and airborne campaigns for ocean, land, ice, and snow techniques: application to the GOLD-RTR data sets. Radio Sci. 46.

Champollion, C., Masson, F., Bouin, M.-N., Walpersdorf, A., Doerflinger, E., Bock, O., Van Baelen, J., 2005. GPS water vapour tomography: preliminary results from the ESCOMPTE field experiment. Atmos. Res. 74, 253–274.

Dach, R., Hugentobler, U., Fridez, P., Meindl, M., 2007. Bernese GPS Software Version 5.0, vol. 640. Astron. Institute, Univ. Bern, Bern, Switz, p. 114.

Degaleesan, S., Dudukovic, M., Pan, Y., 2001. Experimental study of gas-induced liquid-flow structures in bubble columns. AIChE J. 47, 1913–1931.

Elfving, T., Nikazad, T., Hansen, P.C., 2010. Semi-convergence and relaxation parameters for a class of SIRT algorithms. Electron. Trans. Numer. Anal. 37, 321–336.

Eresmaa, R., Järvinen, H., 2006. An observation operator for ground-based GPS slant delays. Tellus Dyn. Meteorol. Oceanogr. 58, 131–140.

Fabra, F., 2013. GNSS-R as a Source of Opportunity for Remote Sensing of the Cryosphere. Univ. Politècnica Catalunya.

Flores, A., 1999. Atmospheric Tomography Using Satellite Radio Signals (PhD Dis).

Flores, A., De Arellano, J.-G., Gradinarsky, L.P., Rius, A., 2001. Tomography of the lower troposphere using a small dense network of GPS receivers. IEEE Trans. Geosci. Rem. Sens. 39, 439–447.

Guerova, G., Jones, J., Douša, J., Dick, G., Haan, S. de, Pottiaux, E., Bock, O., Pacione, R., Elgered, G., Vedel, H., 2016. Review of the state of the art and future prospects of the ground-based GNSS meteorology in Europe. Atmos. Meas. Tech. 9, 5385–5406.

Haji-Aghajany, S., Amerian, Y., Verhagen, S., Rohm, W., Ma, H., 2020. An optimal troposphere tomography technique using the WRF model outputs and topography of the area. Rem. Sens. 12, 1442.

Heublein, M.S.M.E.A., 2019. GNSS and InSAR based water vapor tomography: a Compressive Sensing solution.

Heublein, M., Zhu, X.X., Alshawaf, F., Mayer, M., Bamler, R., Hinz, S., 2015. Compressive sensing for neutrospheric water vapor tomography using GNSS and InSAR observations. 2015 IEEE International Geoscience and Remote Sensing Symposium (IGARSS). IEEE, pp. 5268–5271.

Hirahara, K., 2000. Local GPS tropospheric tomography. Earth, planets Sp. 52, 935–939.

Katzberg, S.J., Torres, O., Grant, M.S., Masters, D., 2006. Utilizing calibrated GPS reflected signals to estimate soil reflectivity and dielectric constant: results from SMEX02. Remote Sens. Environ. 100, 17–28.

Landweber, L., 1951. An iteration formula for Fredholm integral equations of the first kind. Am. J. Math. 73, 615–624.

Larson, K.M., Ray, R.D., Nievinski, F.G., Freymueller, J.T., 2013. The accidental tide gauge: a GPS reflection case study from Kachemak Bay, Alaska. Geosci. Rem. Sens. Lett. IEEE 10, 1200–1204.

Martin-Neira, M., 1993. A passive reflectometry and interferometry system (PARIS): application to ocean altimetry. ESA J 17, 331–355.

Menke, W., 2018. Geophysical Data Analysis: Discrete Inverse Theory. Academic press.

Möller, G., 2017. Reconstruction of 3D Wet Refractivity Fields in the Lower Atmosphere: along Bended GNSS Signal Paths. Südwestdeutscher Verlag für Hochschulschriften.

Pallarés, J.M., Ruffini, G., Ruffini, L., 2005. Ionospheric tomography using GNSS reflections. IEEE Trans. Geosci. Rem. Sens. 43, 321–326.

Rius, A., Cardellach, E., Martin-Neira, M., 2010. Altimetric analysis of the sea-surface GPS-reflected signals. IEEE Trans. Geosci. Rem. Sens. 48, 2119–2127.

Rius, A., Nogués-Correig, O., Ribó, S., Cardellach, E., Oliveras, S., Valencia, E., Park, H., Tarongí, J.M., Camps, A., van der Marel, H., 2012. Altimetry with GNSS-R interferometry: first proof of concept experiment. GPS Solut. 16, 231–241.

Rodriguez-Alvarez, N., Camps, A., Vall-Llossera, M., Bosch-Lluis, X., Monerris, A., Ramos-Perez, I., Valencia, E., Marchan-Hernandez, J.F., Martinez-Fernandez, J., Baroncini-Turricchia, G., 2010. Land geophysical parameters retrieval using the interference pattern GNSS-R technique. IEEE Trans. Geosci. Rem. Sens. 49, 71–84.

Rohm, W., Bosy, J., 2009. Local tomography troposphere model over mountains area. Atmos. Res. 93, 777–783.

Rohm, W., Zhang, K., Bosy, J., 2014. Limited constraint, robust Kalman filtering for GNSS troposphere tomography. Atmos. Meas. Tech. 7, 1475–1486.

Roussel, N., Frappart, F., Ramillien, G., Darrozes, J., Desjardins, C., Gegout, P., Pérosanz, F., Biancale, R., 2014. Simulations of Direct and Reflected Wave Trajectories for Ground-Based GNSS-R Experiments.

Ruffini, n G., Soulat, F., Caparrini, M., Germain, O., Martín-Neira, M., 2004. The Eddy Experiment: accurate GNSS-R ocean altimetry from low altitude aircraft. Geophys. Res. Lett. 31.

Seeber, G., 2003. Satellite Geodesy: Foundations, Methods, and Applications. Walter de Gruyter.

Semmling, A.M., Beyerle, G., Stosius, R., Dick, G., Wickert, J., Fabra, F., Cardellach, E., Ribó, S., Rius, A., Helm, A., 2011. Detection of Arctic Ocean tides using interferometric GNSS-R signals. Geophys. Res. Lett. 38, L04103 https://doi.org/10.1029/2010GL046005.

Semmling, A.M., Beckheinrich, J., Wickert, J., Beyerle, G., Schön, S., Fabra, F., Pflug, H., He, K., Schwabe, J., Scheinert, M., 2014. Sea surface topography retrieved from GNSS reflectometry phase data of the GEOHALO flight mission. Geophys. Res. Lett. 41, 954–960.

Shafei, M.J., Mashhadi-Hossainali, M., 2018. Application of the GNSS-R in tomographic sounding of the Earth atmosphere. Adv. Space Res. 62, 71–83.

Shangguan, M., Bender, M., Ramatschi, M., Dick, G., Wickert, J., Raabe, A., Galas, R., 2013. GPS tomography: validation of reconstructed 3-D humidity fields with radiosonde profiles. Annales Geophysicae. Copernicus Publications (EGU), pp. 1491–1505.

Song, S., Zhu, W., Ding, J., Peng, J., 2006. 3D water-vapor tomography with Shanghai GPS network to improve forecasted moisture field. Chin. Sci. Bull. 51, 607–614.

Troller, M., Geiger, A., Brockmann, E., Bettems, J.-M., Bürki, B., Kahle, H.-G., 2006. Tomographic determination of the spatial distribution of water vapor using GPS observations. Adv. Space Res. 37, 2211–2217.

Xia, P., Cai, C., Liu, Z., 2013. GNSS troposphere tomography based on two-step reconstructions using GPS observations and COSMIC profiles. Annales Geophysicae. Copernicus Publications on behalf of the European, pp. 1805–1815.

Yao, Y., Zhao, Q., 2016. Maximally using GPS observation for water vapor tomography. IEEE Trans. Geosci. Rem. Sens. 54, 7185–7196.

Yao, Y., Zhao, Q., 2017. A novel, optimized approach of voxel division for water vapor tomography. Meteorol. Atmos. Phys. 129, 57–70.

Ye, S., Xia, P., Cai, C., 2016. Optimization of GPS water vapor tomography technique with radiosonde and COSMIC historical data. Ann. Geophys. 34, 789–799.

Zavorotny, V.U., Voronovich, A.G., 2000. Scattering of GPS signals from the ocean with wind remote sensing application. IEEE Trans. Geosci. Rem. Sens. 38, 951–964.

Zhao, Q., Yao, Y., 2017. An improved troposphere tomographic approach considering the signals coming from the side face of the tomographic area. Annales Geophysicae, pp. 87–95. Copernicus GmbH.

Zhao, Q., Yao, Y., Yao, W., Xia, P., 2018. An optimal tropospheric tomography approach with the support of an auxiliary area. Annales Geophysicae, pp. 1037–1046. Copernicus GmbH.

Zhao, Q., Zhang, K., Yao, Y., Li, X., 2019. A new troposphere tomography algorithm with a truncation factor model (TFM) for GNSS networks. GPS Solut. 23, 64.

Zhao, Q., Yao, W., Yao, Y., Li, X., 2020. An improved GNSS tropospheric tomography method with the GPT2w model. GPS Solut. 24, 1–13.